PAPER • OPEN ACCESS

Improving a two-equation eddy-viscosity turbulence model to predict the aerodynamic performance of thick wind turbine airfoils

To cite this article: Galih Bangga *et al* 2018 *J. Phys.: Conf. Ser.* **974** 012019

View the article online for updates and enhancements.

Related content

- Experimental Measurement and CFD Model Development of Thick Wind Turbine Airfoils with Leading Edge Erosion
David C. Maniaci, Edward B. White, Benjamin Wilcox et al.

- Aerodynamic Analysis of Trailing Edge Enlarged Wind Turbine Airfoils
Haoran Xu, Wenzhong Shen, Weijun Zhu et al.

- Influence of hinge point on flexible flap aerodynamic performance
H Y Zhao, Z Ye, P Wu et al.

Improving a two-equation eddy-viscosity turbulence model to predict the aerodynamic performance of thick wind turbine airfoils

Galih Bangga[1,2]**, Tri Kusumadewi**[3]**, Go Hutomo**[4]**, Ahmad Sabila**[5]**, Taurista Syawitri**[6]**, Herlambang Setiadi**[7]**, Muhamad Faisal**[8,9]**, Raditya Wiranegara**[10]**, Yongki Hendranata**[11]**, Dwi Lastomo**[12]**, Louis Putra**[13] **and Stefanus Kristiadi**[14]

[1] Institute of Aerodynamics and Gas Dynamics, University of Stuttgart, Stuttgart, Germany
[2] Mechanical Engineering Department, Institut Teknologi Sepuluh Nopember, Surabaya, Indonesia
[3] School of Manufacturing System and Mechanical Engineering, Sirindhorn International Institute of Technology, Thammasat University, Thailand
[4] Toyota SO Department, Astra International, Ltd., Indonesia
[5] Civil Engineering Department, Universitas Brawijaya, Malang, Indonesia
[6] Mechanical Engineering Department, Universitas Muhammadiyah Surakarta, Surakarta, Indonesia
[7] School of Information Technology & Electrical Engineering, The University of Queensland, Brisbane, Australia
[8] Non-Installation Top Range Department, Berca Schindler Lifts, Ltd., Indonesia
[9] Graduate Institute of Automation and Control, National Taiwan University of Science and Technology, Taiwan
[10] School of Aerospace, Transport and Manufacturing, Cranfield University, United Kingdom
[11] Mechanical Engineering Department, Texas A&M University, College Station, United States
[12] PUI-PT Mechatronics and Industrial Automation Research Center, Intitut Teknologi Sepuluh Nopember, Surabaya, Indonesia
[13] Mechanical Engineering Department, Politecnico di Milano, Milan, Italy
[14] Aeronautics Department, Imperial College of Science, Technology and Medicine, London, United Kingdom

E-mail: `bangga@iag.uni-stuttgart.de` and `galih.bangga90@gmail.com`

Abstract. Numerical simulations for relatively thick airfoils are carried out in the present studies. An attempt to improve the accuracy of the numerical predictions is done by adjusting the turbulent viscosity of the eddy-viscosity Menter Shear-Stress-Transport (SST) model. The modification involves the addition of a damping factor on the wall-bounded flows incorporating the ratio of the turbulent kinetic energy to its specific dissipation rate for separation detection. The results are compared with available experimental data and CFD simulations using the original Menter SST model. The present model improves the lift polar prediction even though the stall angle is still overestimated. The improvement is caused by the better prediction of separated flow under a strong adverse pressure gradient. The results show that the Reynolds stresses are damped near the wall causing variation of the logarithmic velocity profiles.

1. Introduction

Flow separation has become the subject of interest for many years due to its importance in practical engineering problems especially for lifting structures or airfoils. Unfortunately, these lifting devices often attain optimum performance at the condition of "onset of separation" which implies that separation phenomena must be well understood if the analysis is aimed at practical applications [1]. The separation process can be explained by the change of pressure gradient occurring on the airfoil surface. It happens when the angle of incidence of the incoming flow increases, which results in an augmentation of the pressure gradient especially on the suction side of the airfoil. This causes flow detachment resulting in a significant loss of the aerodynamic performance. Rhie and Chow [1] described that this condition involves a strong interaction between the viscous flow and the inviscid flow outside of the boundary layer. On the other hand, in the linear lift region where the flow is attached, the interaction is significantly weaker. This indicates that viscous effects are important and need to be considered for the flow experiencing a large adverse pressure.

Wind turbines often operate at over-rated wind speed or pitch-fault conditions. These issues increase the local angle of attack and pressure gradient occurring on the surface. As a result, stronger separation is expected to occur. These phenomena become more severe if the inboard blade area is considered because the local inflow angle is usually very high due to limitation of the twist angle by structural constraints [2]. Furthermore, as the rotor size increases vastly nowadays, thicker airfoils need to be used from the inboard area extending further outboard longer than more conventional rotors which even enhance the adverse pressure gradient occurring on the blade sections. It is clear that the rotor becomes more vulnerable towards flow separation, and this implies that accurate predictions of flow separation are important for wind turbine aerodynamics.

Due to complexity of the issue, one effective way to bring the physics into numerical approach is to employ a large scale computation using the Navier-Stokes equations. These computational fluid dynamics methods (CFD) have been applied in many engineering problems involving the prediction of flow over wind turbines [3–7]. However, due to the lack of robust CFD methods, most CFD studies were done focusing only on the validation of the CFD codes rather than the physical phenomena of the flow. It is already well known that the Reynolds Averaged Navier - Stokes (RANS) method, commonly used to treat the flow turbulence, is inaccurate for massively separated flows. The maximum lift coefficient and post stall behaviour of airfoils were reported not to be sufficiently captured [8]. Applying eddy-resolving models like Large Eddy Simulations (LES) or Detached Eddy Simulations (DES) has been shown to improve the situation [8–11]. It has been demonstrated that RANS had difficulty in predicting the stall characteristics of some airfoils, while the LES based simulations were able to deliver accurate predictions. However, due to the 3D nature of eddies, computations should be carried out in three dimensional configuration. For this purpose, two dimensional simulations can not be used and this can be quite an issue if a lot of computations need to be performed like in generating airfoil databases for preparation of the Blade Element Momentum (BEM) model [12]. It is always possible to develop the airfoil databases using DES only for the high angle of attack cases where separation presents (using 3D grid) while the standard RANS approach or even XFOIL can be applied for the lower angle of attack (2D grid is applicable). However, the the grids should be sufficiently small to resolve the inertial scales of turbulence. The problem arises when this approach is used for the inboard wind turbine airfoil because the relative thickness of the airfoil is greater than 35%. As a consequence, no linear region presents and separation occurs for the whole range of the angle of attack.

In the URANS approach, the turbulent closure is modeled by assuming the "eddy" viscosity as a function of the "laminar" viscosity. In fact, actually eddy viscosity is not physical and is generated based on a simple relation called Boussinesq hypothesis. The idea is to relate the

turbulence stresses to the mean flow in order to close the URANS equations by modeling the Reynolds stress terms. Therefore, turbulence models based on this theorem is usually called the eddy-viscosity turbulence models (EVTM). It has been agreed that it is too dangerous to assume validity of a turbulence model for a wide variety of flows. Many authors have developed improved models for the RANS approach. Myong and Kasagi [13] extended the original $k - \varepsilon$ model considering the two characteristic length scales for the dissipation rate, one very near the wall and the other remote from the wall, which are related to the transfer of the turbulent momentum. The new approach was able to correctly model the wall-limiting behaviour of the major turbulence quantities for the case of fully developed turbulent pipe and channel flows. One of the most striking contribution was given by Menter [14] in combining the Wilcox $k - \omega$ model [15] with the standard $k - \varepsilon$ model according to Launder and Spalding [16]. The model reduces the freestream sensitivity of the Wilcox model while maintaining a good prediction for wall bounded flows. In 2001, Nagano and Hattori [17] developed an improved model based on a low Reynolds number non-linear $k - \varepsilon$ model flow in a rotating channel. Chitsomboon and Thamthae [18] and Bangga et al. [19, 20] have documented that modifications of the eddy viscosity parameter can lead to a more accurate flow prediction, especially if massive flow separation is encountered. In fact, most of turbulence models tune the relation of the eddy viscosity parameter in their development. Based on these insights, the present studies aim to improve CFD predictions of wind turbine airfoils by modifying the turbulent viscosty of a two-equation Unsteady-RANS (URANS) turbulence model. In this case, unsteady simulations are chosen because the resulting flow field of airfoils under massive separation is always unsteady.

A damping factor is introduced in the turbulent viscosity equation for the Menter SST turbulence model [14]. This model is chosen because it is one of the most commonly used turbulence models in industry, and reasonably accurate to predict flows experiencing a strong adverse pressure gradient. The main idea behind the modification is to reduce the contribution of the Reynolds stress terms to the flow near wall region. The modification incorporates the ratio between the the turbulent kinetic energy to its specific dissipation for separation detection. The goal is to activate the modification for separated flow while minimizing the impact for the attached flow case.

The paper is organized as follows. The test case and numerical procedures are given in Section 2. Section 3 presents the results, and the conclusion is made in Section 4.

2. Methods
2.1. Adjustment of the turbulence model
The present section describes the governing equation of the adjusted turbulence model. The Menter SST [14] turbulence model is selected because the model is well known to provide reasonable accuracy for RANS based simulations under strong adverse pressure gradient flows. The original model was proposed by Menter and has become the most used EVTM since then. The approach combines the "standard" $k - \varepsilon$ [16] in the free shear flows and the Wilcox $k - \omega$ [21] in the wall bounded area to reduce the sensitivity of the $k - \omega$ model towards the inflow conditions. This is done by transforming the $k - \varepsilon$ equations to the equivalent $k - \omega$ based through the blending functions F_1 and F_2. They are unity in the near-wall area activating the standard k- ω model, and zero far away from the surface enforcing the transformed k- ε model to be activated. In addition, the SST model introduces a damped cross-diffusion derivative term for the ω equation and revises the definition of the turbulent viscosity to account for the turbulent shear stress transport. These features make the SST model more accurate and reliable than the Wilcox $k - \omega$ in many cases.

The model is governed by two transport equations, one for turbulent kinetic energy (k) and one for its specific dissipation rate (ω), which can also be thought of as the ratio of ε to k. It is a semi-empirical model combining the exact equation for k and non-exact formulation for ε. The

equation for the specific dissipation rate is governed using physical reasoning and bears little resemblance to its mathematically exact counterpart. The transport equations for k and ω are given in Equations (1) and (2), respectively.

$$\frac{\partial}{\partial t}(\rho k) + \frac{\partial}{\partial x_i}(\rho k u_i) = \frac{\partial}{\partial x_j}\left(\Gamma_k \frac{\partial k}{\partial x_j}\right) + \tilde{G}_k - Y_k + S_k \tag{1}$$

$$\frac{\partial}{\partial t}(\rho \omega) + \frac{\partial}{\partial x_i}(\rho \omega u_i) = \frac{\partial}{\partial x_j}\left(\Gamma_\omega \frac{\partial \omega}{\partial x_j}\right) + G_\omega - Y_\omega + D_\omega + S_\omega . \tag{2}$$

G_ω and $\tilde{G}_k$ represent the generations of ω and the turbulence kinetic energy due to mean velocity gradients, respectively, while Y_k and Y_ω represent the dissipations of k and ω due to turbulence, respectively [22]. The blending of the standard $k - \varepsilon$ model with the Wilcox $k - \omega$ models is facilitated by the blending functions, F_1 and F_2, which introduce a cross-diffusion term D_ω. The effective diffusivities are given by

$$\Gamma_k = \mu + \frac{\mu_t}{\sigma_k} \tag{3}$$

$$\Gamma_\omega = \mu + \frac{\mu_t}{\sigma_\omega} , \tag{4}$$

where σ_k and σ_ω are the turbulent Prandtl numbers for k and ω, respectively [22]. μ is the dynamic viscosity and μ_t is the turbulent viscosity which is defined as

$$\mu_t = \frac{\rho k}{\omega} \frac{1}{\max\left[\frac{1}{\alpha^*}, \frac{SF_2}{a_1 \omega}\right]}. \tag{5}$$

S defines the strain rate magnitude. For high Reynolds number flows, a_1 is equal to 0.31 and α^* is unity .

It has been shown by Chitsomboon and Thamthae [18] and Bangga et al. [19, 20] that the modification of the turbulent viscosity near the wall can improve CFD predictions of airfoils. The modifications employed a damping function implemented in the eddy viscosity formulation. Both the approaches in [18] and in [19, 20] assumed that μ_t depends on the wall distance. The modification of μ_t by Chitsomboon and Thamthae [18] is:

$$\mu_t^* = \left\{0.1 + \left[1 - 0.1\mathrm{tanh}\left((0.03y^+)^4\right)\right]\left[0.9 + 0.1\mathrm{tanh}\left((0.005y^+)^8\right)\right]\right\}\mu_t, \tag{6}$$

and according to Bangga et al. [19, 20] (for the $k - \varepsilon$ turbulence model) is

$$\mu_t = f_b \rho C_\mu \frac{k^2}{\varepsilon}, \tag{7}$$

$$f_b = f C_b, \tag{8}$$

where

$$C_b = \frac{1000}{A_0 + A_1 \frac{kU^*}{\varepsilon}} \tag{9}$$

with

$$U^* = \sqrt{S_{ij} S_{ij} + \tilde{\Omega}_{ij} \tilde{\Omega}_{ij}} \tag{10}$$

$$\tilde{\Omega}_{ij} = S_{ij} - 2\varepsilon_{ijk}\omega_k \tag{11}$$

$$S_{ij} = \frac{1}{2}\left(\frac{\partial u_j}{\partial x_i} + \frac{\partial u_i}{\partial x_j}\right). \tag{12}$$

The value of f is damped on the buffer zone around $5 < y^+ < 30$ and is unity on the other zones. Further details of the modification can be seen in [19, 20].

The main objective of the turbulent viscosity modification is to reduce the Reynolds stresses contribution of the turbulence model. By doing so, the ability of the flow to withstand separation reduces. This is helpful to facilitate the simulation in predicting stronger separation (that is usually underestimated). However, it shall be noted that the modified model shall not destroy the basic calibration case for flows without adverse pressure gradient like the flow over a flat plate. Based on the similar idea as in [18–20], the present study also introduces a simple modification by adding a damping factor for the turbulent viscosity equation. The equation for the turbulent viscosity is redefined as

$$\mu_t^* = f_b \mu_t \tag{13}$$

In Equation (13), μ_t^* is the newly defined turbulent viscosity that is damped by parameter f_b with the condition

$$f_b = \begin{cases} < 1, & \text{if } \sqrt{k}/(0.09\omega y) > w_d \\ 1, & \text{otherwise} \end{cases} \tag{14}$$

In Equation (14), y represents the wall distance. The idea is that the damping factor is less than unity, *i.e.,* reducing the turbulent viscosity, if the dimensionless property of the inverse wall distance, $\sqrt{k}/(0.09\omega y)$, is larger than a specific wall distance constant defined as w_d. Physically, this means that the turbulent viscosity is being reduced by Equation (14) approaching the wall. It is shown from Equation (14) that f_b acts as a step fuction, similar to those employed in [18–20]. The discussion about the impact of this parameter will be given in section 3.3. The present modification is indeed simpler than the one employed by Bangga et al. [19,20] for the $k-\varepsilon$ turbulence model. This is done to facilitate faster convergence than the previous implemented approaches. Furthermore, the definition of the wall distance is not directly obtained from y^+ but instead employing the connection between the $\sqrt{k}/(0.09\omega y)$ ratio. This usage is intended for a better detection of separation (based on k and ω) rather than purely y^+. It shall be noted that noticeable magnitude of $\sqrt{k}/\omega$ occurs within the separation area.

2.2. Computational mesh and numerical methods
Two dimensional numerical simulations have been carried out using a CFD code, FLOWer, from the German Aerospace Center (DLR) [23–25] employing the Unsteady Reynolds-Averaged Navier-Stokes (URANS) approaches. During the last years, the code was continuously extended at the Institute of Aerodynamics and Gas Dynamics - University of Stuttgart for wind turbine applications [26, 27]. The numerical procedure of the FLOWer code is based on structured meshes. The spatial discretization scheme used in the present study is a central cell-centered finite volume formulation because it provides high robustness and is well-suited for parallel applications [24]. The method employs the Jameson-Schmidt-Turkel (JST) [28] approach for flux computations. The scheme is second order accurate in space on smooth meshes. The method utilizes central space discretization with artificial viscosity and explicit hybrid 5-stage Runge-Kutta time-stepping schemes. Dual time-stepping according to Jameson [29] with second-order accuracy in time, multi-grid level 3 and the implicit residual smoothing with variable coefficients
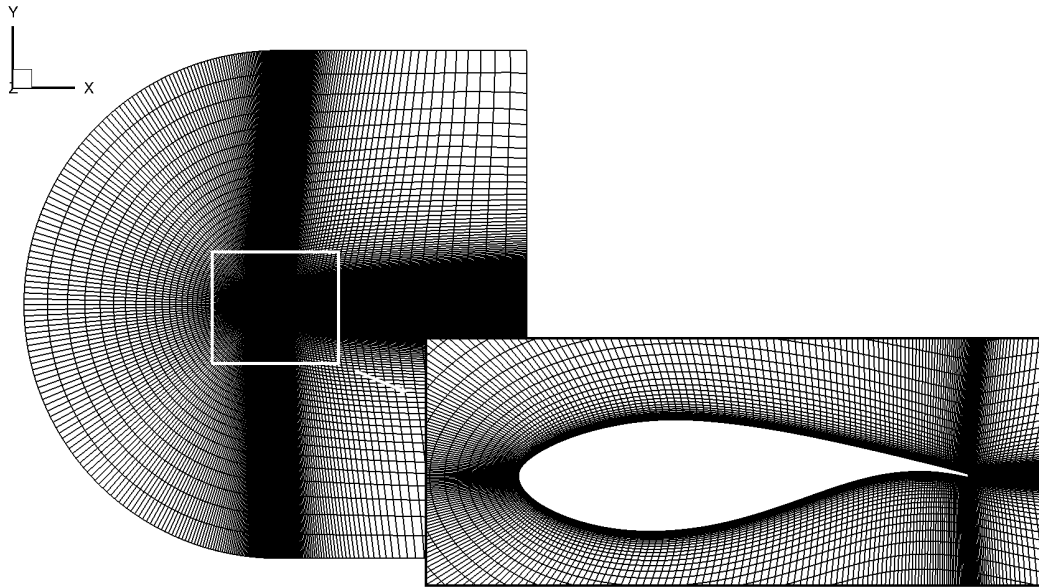
Figure 1: Computational mesh used in the present CFD calculations.

according to Radespiel *et al.* [30] were applied. All simulations were performed by considering the flow unsteadiness with the time step value less than 2% of the time required for a fluid particle convecting over the airfoil, defined as

$$\Delta t < \frac{2}{100} \frac{c}{U_\infty} \; , \tag{15}$$

where U_∞ is the freestream velocity and c is the chord length. Basic sensitivity studies concerning the temporal and spatial resolutions will be given in Section 3.1.

The mesh of the airfoil was generated using an automated script developed at IAG using the grid generator IGG. The domain is C-H type extending 50 times chord length in all directions. The structured mesh is intensively refined near the airfoil wall, see Figure 1. The distance of the first cell layer was set to meet the non-dimensional wall distance of $y^+ < 1$. As no wall function is used, maintaining y^+ lower than unity is important to properly resolve the laminar sub-layer region near the wall. The resolution of the grid consists of 280 and 128 cells in streamwise and wall normal directions, respectively, and among them 32 cells are located within the boundary layer.

2.3. The airfoils

In the present studies, four different wind turbine airfoils designed at the Delft University of Technology, namely DU 91-W2-250 (25% relative thickness), DU 97-W-300 (30%), DU 00-W2-350 (35%) and DU 00-W2-401 (40%) are considered. The description of the airfoil nomenclature was given in [31]. DU stands for Delft University and followed by the year in which the airfoil was designed. The letter W represents that the airfoil is used for wind energy application where the additional number following it indicates that there has been more than one airfoil design with the same thickness that year. The last digits of the nomenclature represent 10 times of the relative thickness percentage. A good review of the airfoils performance and their sensitivity towards surface roughness can be found in [31, 32].

The airfoils were measured in the Delft University wind tunnel (LST) and in the laminar wind tunnel at IAG. The measurement was carried out at a Reynolds number of $Re = 3$ million. In this

Table 1: Operating condition of the measurements.

Airfoil name	Re [million]	Trip location [%]
DU 91-W2-250	3.0	5% SS
DU 97-W300	3.0	5% SS, 20% PS
DU 00-W2-350	3.0	2% SS, 10% PS
DU 00-W2-401	3.0	2% SS, 10% PS

campaign, turbulators were employed on the airfoil surfaces to evaluate its performance under soiled conditions. Detailed information of the trip locations is given in Table 1. In the CFD simulations, the transition was prescribed at turbulator position, *i.e.*, turbulence production was switched-on at this location. For the DU 91-W2-250 airfoil, the boundary layer tripping was introduced only on the suction side at $x/c = 5\%$. The transition location on the pressure side was estimated using XFOIL [33] for each angle of attack, resulting in 20 different transition location data. For the airfoil with 30% relative thickness, DU 97-W300 airfoil, the location of trip in the CFD simulation is at the relative chordwise positions of 5% and 20% on the suction and pressure sides, respectively. The relative thicknesses of the examined thicker DU airfoils, DU 00-W2-350 and DU 00-W2-401 airfoils, are 35% and 40%, respectively. On these airfoils, the boundary layer tripping at $x/c = 2\%$ and 10% on the suction and pressure sides, respectively, was applied. In addition to that, CFD computations for fully turbulent boundary layer were also performed for comparison.

3. Results and discussion
3.1. Temporal and spatial discretization studies
Before the examinations are carried out, it is necessary to verify the consistency of the employed CFD model. In this section, basic sensitivity studies for the temporal and spatial discretizations are presented. The test was performed on the DU 91-W2-250 airfoil operating at a very high Reynolds number (Re) of 17.6 million. This high Re condition was purposely chosen because this airfoil is commonly used for the application of large wind turbines in range of 10-20 MW like the AVATAR rotor [34]. The employed turbulence model is the Menter SST $k - \omega$ and no laminar-turbulence prediction/prescription was applied in this grid study, *i.e.*, fully turbulent computations.

The time step size for the present 2D simulations is Δ_t 0.00035 s, corresponding to 1.66% of the convective time of a fluid particle passing the airfoil. The definition of the convective time can be seen in Equation (15). To demonstrate that this time step size is sufficient, an additional CFD simulation at $\alpha = 14°$ was carried out employing a smaller relative time step size of $\Delta_t = 0.4\%$. Figure 2 shows that reducing the time step does not bring a significant influence on the results. This implies that the CFD simulations using the basic time step size of $\Delta_t = 1.66\%$ are plausible.

A grid study was performed in order to show that the numerical results are independent of the number of grid cells. Three different streamwise grid densities were examined; Grid 1: 200 cells, Grid 2: 280 cells, Grid 3: 360 cells. The results of the grid studies are presented in Figure 3. It is shown that the increased grid resolutions hardly produce any differences in both the lift and drag polars for a wide range of angles of attack (α), inferring that the grid is spatially converged. All the grid resolutions generally are in a good agreement within the linear lift region but Grid 1 slightly underestimates the results in the post stall regimes, both in positive and negative stall angles. Considering the accuracy and computational cost, Grid 2 with the streamwise resolution of 280 cells is used in all further simulations.
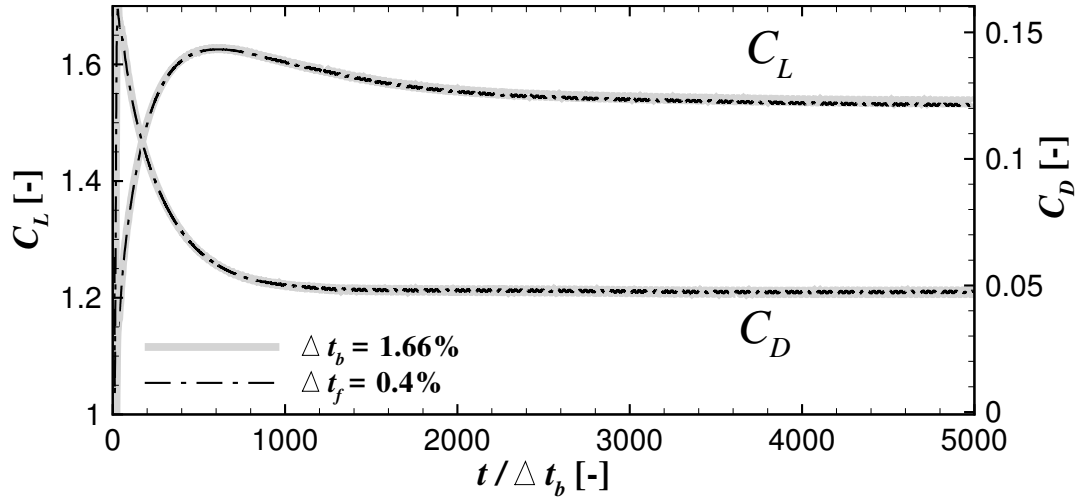
Figure 2: The effect of temporal discretization on the predicted aerodynamic coefficients. The simulations were carried out for the DU 91-W2-250 airfoil, at $\alpha = 14°$ and $Re = 17.6 \times 10^6$, for the baseline ($\Delta t_b = 1.66\%$) and fine ($\Delta t_f = 0.4\%$) time steps.
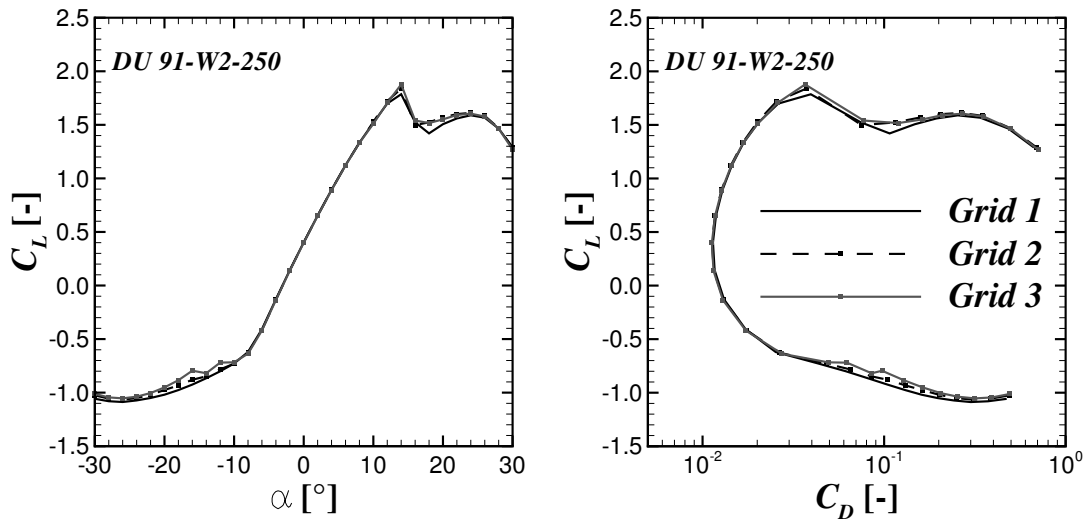

Figure 3: Computed lift and drag polars using three examined grid densities. The increased grid density hardly influences the CFD results.

3.2. Effects of the Reynolds number and transition location

Despite the use for large turbine blades, the measurement data for this airfoil is only available at Re of 3 million [32]. The computation at this condition was also carried out using Grid 2 to see the influence of Re. The results for lift and drag coefficients are depicted in Figures 4a and 4b, respectively. Black-squared symbol represents the measurement at $Re = 3 \times 10^6$, dashed-dotted line is for the CFD computation at $Re = 3 \times 10^6$ by applying the turbulator described in Section 2.3, dashed line is for the CFD computation at $Re = 3 \times 10^6$ assuming a fully turbulent boundary layer and solid line is for the CFD computation at $Re = 17.6 \times 10^6$ assuming a fully turbulent boundary layer. It is shown that all the computations over-estimate the maximum

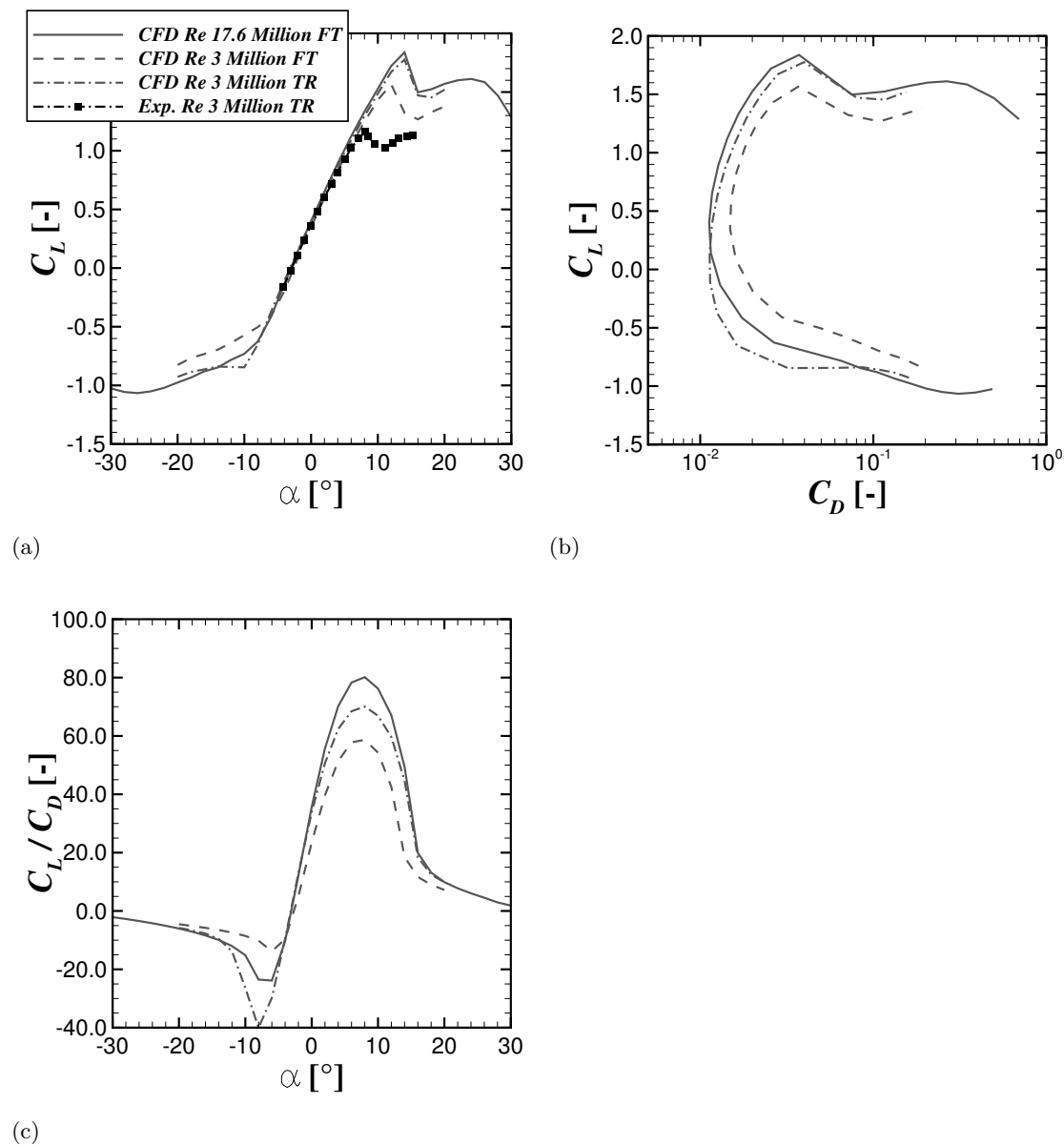(a)   (b)

(c)

Figure 4: The effect of Reynolds number for the DU 91-W2-250 airfoil at fully turbulent (FT) and tripped (TR) conditions. The maximum lift coefficient reduces at smaller Re for fully turbulent boundary layer flow.

lift coefficient, showing the inaccuracy of the original SST model to simulate the aerodynamic characteristics in the post-stall region. It is observed that a higher attained maximum lift can be achieved by the airfoil operating at a larger Reynolds number. For example, the maximum lift coefficient for the case employing $Re = 17.6 \times 10^6$ is about 1.85 at $\alpha = 13.9°$, while it is only about 1.58 at $\alpha = 11.5°$. This indicates that increasing Re can lead to a higher maximum lift and to a noticeable delay of the lift stall. In terms of drag, a remarkable reduction of the drag coefficient is observed for the case operating at a larger Re. This effect seems to occur for the whole range of the studied angles of attack. From Figure 4c, it becomes evident that the airfoil performance enhances considerably with increasing Re. It is shown that the ratio of lift to drag
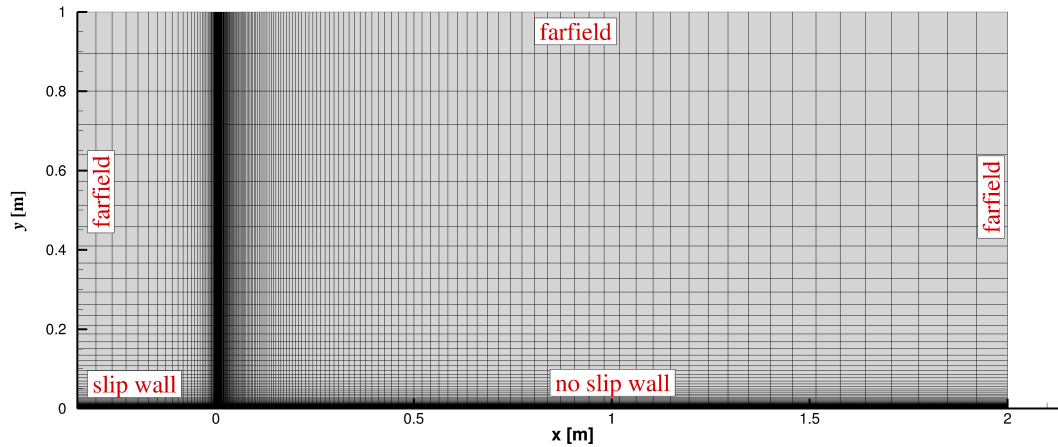
Figure 5: 2D mesh for parametric studies on a flat plate flow. The employed boundary conditions are embedded on the figure.

becomes larger with Re especially approaching its maximum value. It is shown that maximum C_L/C_D for the case at $Re = 3\text{x}10^6$ (FT) is 59 while it reaches 80 for $Re = 17.6\text{x}10^6$.

In Figure 4, it is shown that the location of transition point has a little influence on C_L for the linear lift region. The deviation starts to occur when the angle of attack is higher than $13.9°$, corresponding to the stall angle for the case assuming the fully turbulent boundary layer. It is shown that earlier transition location results in the lower attained maximum lift as well as a smaller lift magnitude in the post-stall area. The transition location seems to have a stronger influence for the drag coefficient. Similarly, the ratio of C_L/C_D also increases for the case employing transitional flows. It is noticed that even though the boundary layer tripping is so close to the leading edge ($< 5\%$), the laminar arc length of the airfoil is long enough to influence the flow field which confirms that thick airfoils are more sensitive towards the location of laminar-turbulent transition.

3.3. Damping factor influence

In this section, parametric studies on the damping effects are given. The modification involves two main parameters: the damping magnitude (f_b) and the wall distance constant (w_d) where the damping is applied. Both parameters give an influence on the resulting flow field. In order to ensure that the modification does not destroy the basic calibration of the original SST model, a careful study needs to be carried out for a problem with a well known solution like for flat plate flows. To do so, an additional mesh was prepared for this purpose as shown in Figure 5. The resolutions of the mesh are of 161 and 97 grid points in streamwise and normal flow directions, respectively. The employed boundary conditions are embedded as well in Figure 5. It shall be noted that the entrance of the flow was set as a slip wall to facilitate better convergence and to allow a better observation of the results downstream this area where a no-slip wall boundary condition was applied. In the interface between these two different wall-type boundary conditions, a significant mesh refinement was conducted allowing a better observation of the flow at a smaller Reynolds number. Despite that, a fully turbulent boundary layer was assumed. Thus, the observation is focused on high Reynolds number flow greater than 1e5. This value is reasonable as the intended purpose of the study is for wind turbine applications. Steady simulations were carried out as no flow separation occurs for a flat plate.

Figure 6 shows the results of the simulations in terms of the skin friction coefficient (C_f) as
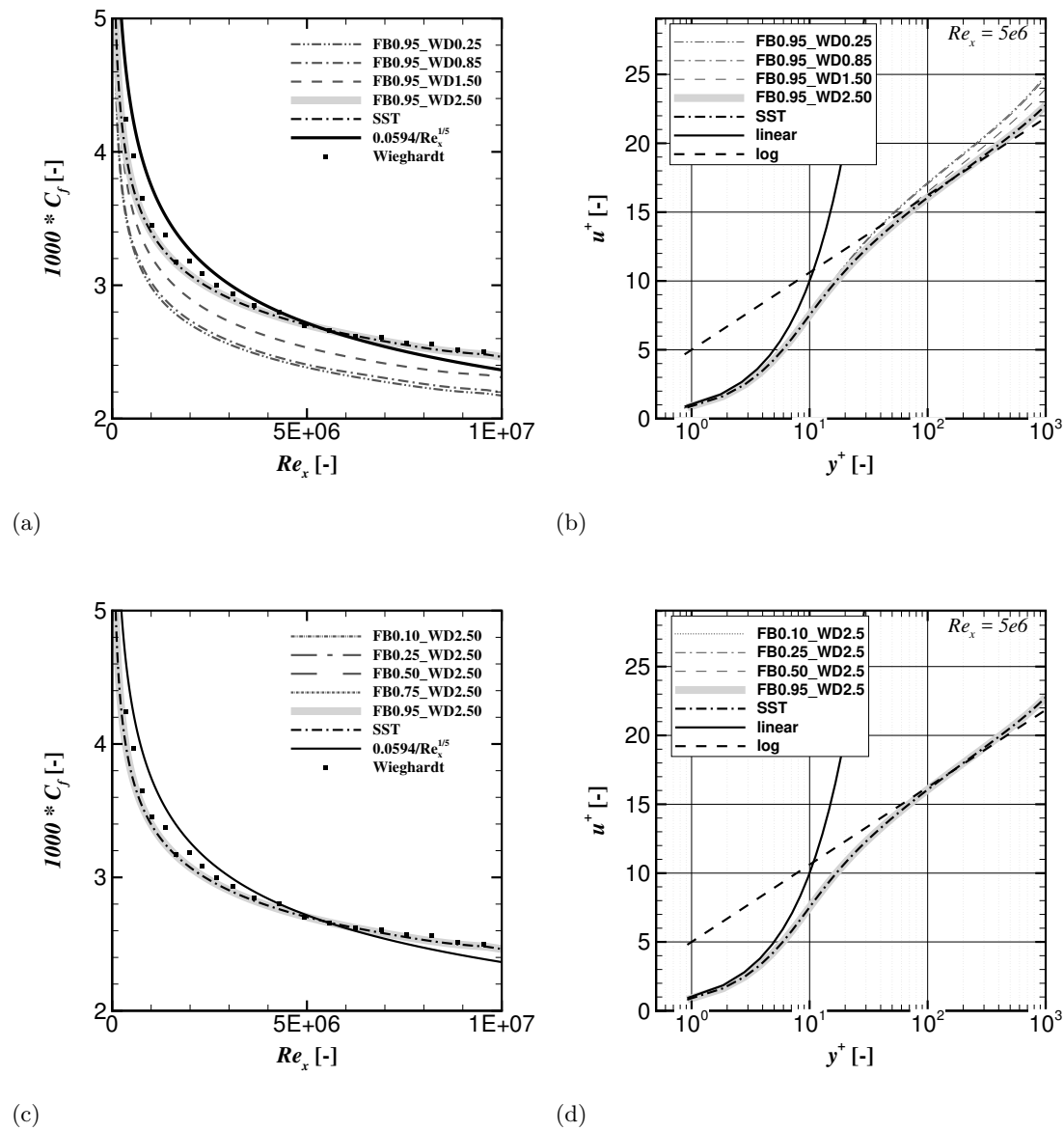
(a)

(b)

(c)

(d)

Figure 6: Sensitivity of modified parameters on flat plate flow. Measurement data for C_f is obtained from [35].

a function of the local streamwise Reynolds number and the logarithmic velocity plot is also presented. In Figures 6a and 6b, the effects of w_d on the flow are assessed. The value of f_b was set to constant ($f_b = 0.95$) in these two figures. It can be seen that C_f is underestimated if w_d is too small. This means that the affected wall distance above the wall is too large. A similar behaviour is observed as well for u^+ within $y^+ > 10$. The model becomes closer to the reference data as w_d increases, and it coincides to each other with the original SST model when w_d reaches 2.5. Thus, this value was set as a reference in assessing the effects of f_b in Figures 6c and 6d. As a consequence, the model still well resembles the original SST results even when f_b is as small as 0.1, please see Figures 6c and 6d.

(a)   (b)

(c)   (d)
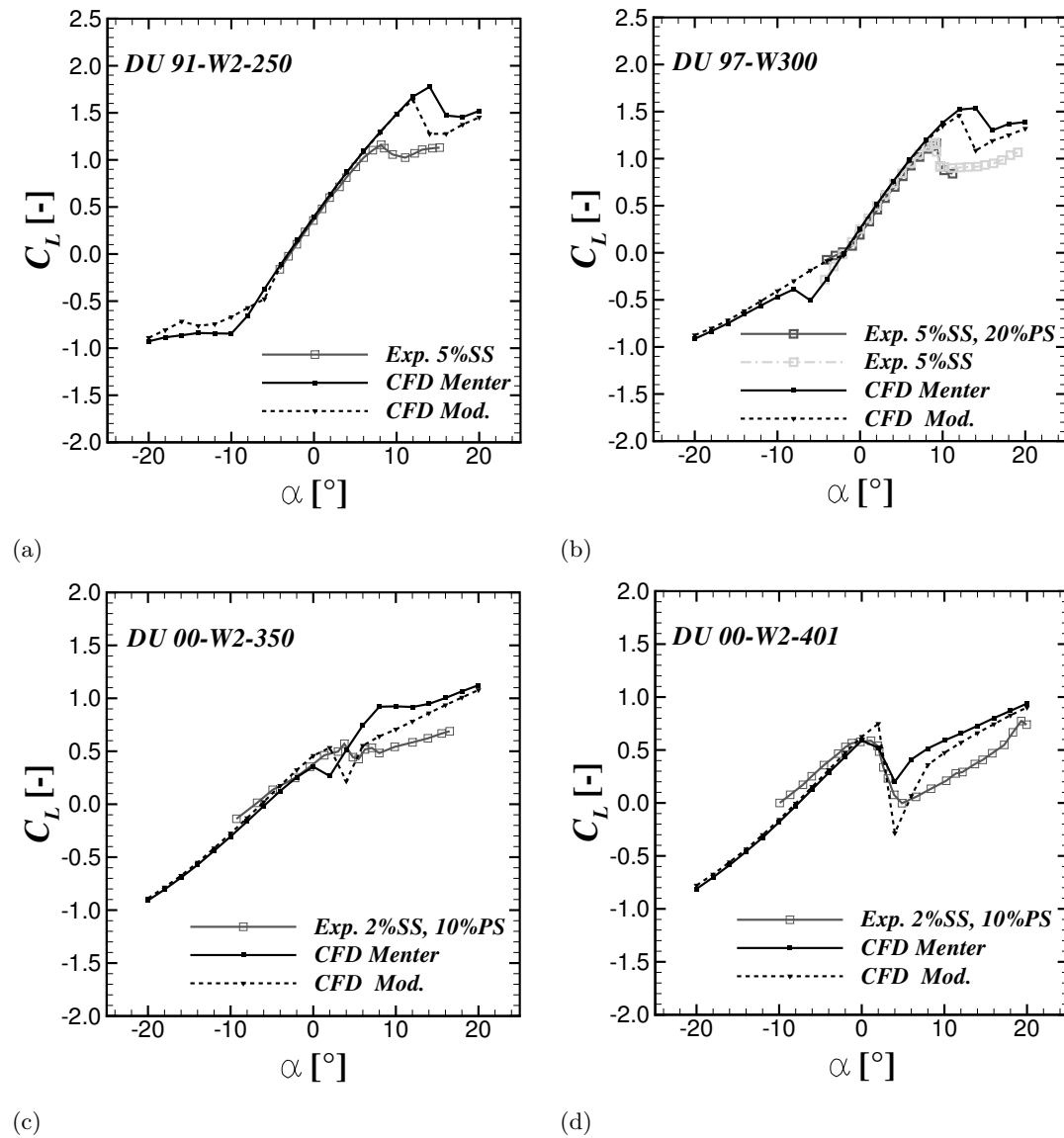
Figure 7: Lift coefficient polar of the four examined DU-airfoils. The adjustment of the turbulent viscosity improves the CFD prediction for these thick wind turbine airfoils.

3.4. Performance of the modified model

The performance of the adjusted turbulence model is examined in this section. The damping factor of $f_b = 0.1$ (with $w_d = 2.5$) was selected according to the consideration described in the previous section. The predicted lift polars from the studied airfoils are compared with measurement data [32] and CFD simulations using the Menter SST turbulence model, depicted in Figure 7. All the numerical computations were carried out according to the measurement data in Table 1. The transition location was prescribed according to the turbulator position in the experiment. Downstream of this location the turbulent generation term was switched-on, ramp-up to 1 within two grid cells. Detailed description on the boundary layer tripping applied in each studied airfoil can be seen in Section 2.3. The studies were performed for a relatively wide angles of attack range, from -20° up to 20°, capturing both the positive and negative stalls.

For each airfoil, the step of α in the simulations is $2°$. This implies that 20 individual simulations are required for each airfoil in each studied turbulence model. In total, 160 simulations were carried out for these four different airfoils.

The results of the CFD computations in terms of the lift coefficient are presented in Figure 7. Symbolized, solid and dashed lines represent the measurement, CFD results with the Menter SST model and with the modified model, respectively. All the CFD models show similar results for the linear lift regime. At higher angles of attack, deviations start to occur as depicted in Figure 7. The modified model seems to reduce the maximum lift coefficient and results in earlier stall, especially for the DU 91-W2-250, DU 97-W-300 and DU 00-W2-350 airfoils, but is less dominant for the DU 00-W2-401 airfoil section. In fact, the maximum lift for the thickest studied airfoil increases slightly as shown in Section 3.3. However, in the post-stall regime, the present model shows consistent results for all the studied airfoils. It can be seen that the addition of the damping factor reduces the lift coefficient predicted by the CFD computations. In general, it is shown that the proposed modification improves the CFD prediction compared to the original model, even though all the models are failed in mimicking the experimental results. Three main reasons may explain this behavior. (1) Flow separation on airfoils at high angles of attack is a complex 3D-unsteady flow phenomenon. Two dimensional URANS computations may not be able to model the flow properly, and 3D computations are expected to improve the situation [36]. (2) As all the turbulent eddies are modeled using URANS, the accuracy of CFD computations depends strongly on the employed model. This implies that the ultimate accuracy of the CFD simulations is the accuracy of the turbulence model itself [37]. The use of eddy resolving approaches like Large Eddy Simulations (LES) or Detached-Eddy Simulations (DES) are believed to better mimic the experiment. (3) The overestimation of the maximum lift seems to be contributed as well by the strong unsteadiness of the flow. It can be clearly seen in Figure 8 that predicted C_L from the modified model drops with increasing simulation time up to around $t/\Delta t = 3000$. Then, C_L increases again as the lift fluctuation presents. This indicates that the accurate prediction can be hindered by a strong unsteady effect. Despite that, the modified model clearly improves the prediction as the lift fluctuation at high angle of attack is captured in comparison to the original SST model which shows no indication of unsteadiness
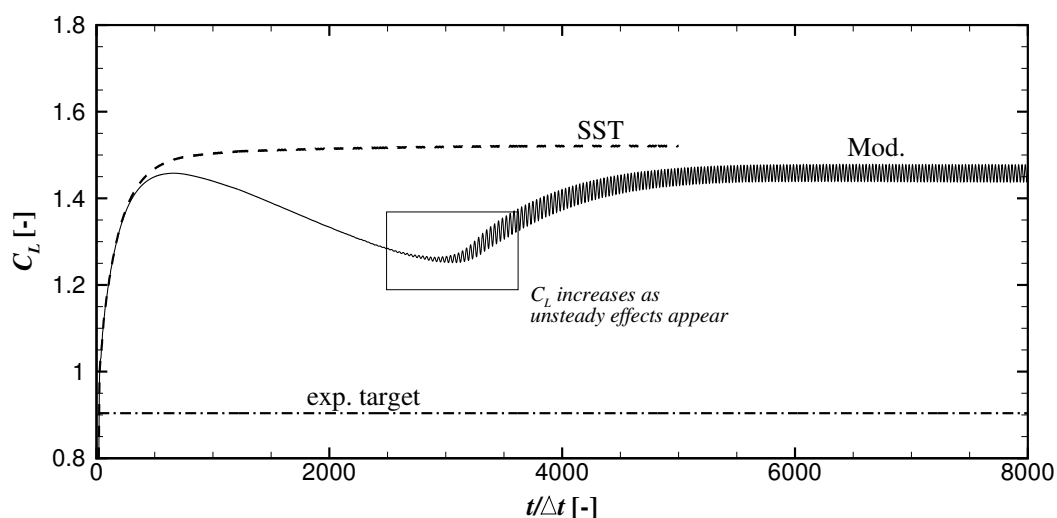

Figure 8: Unsteady effects at maximum lift. The simulations were carried out for the DU 97-W300 airfoil at $\alpha = 12°$.

up to $t/\Delta t = 5000$.

Figures 9a and 9b show the pressure coefficient distributions of the DU 91-W2-250 airfoil at $\alpha = 6°$ and at $\alpha = 14°$. The predicted Cp distribution of the present model coincides with the Menter SST model for the small angle of attack while it deviates strongly at a higher α. It is shown that, for $\alpha = 14°$, the minimum pressure peak becomes more positive in the modified model. This results in the pressure level increase downstream of this position. A slightly lower pressure compared to the Menter SST model is observed only within a small area near the trailing edge. On the pressure side of the airfoil, a small deviation is also observed. It can be seen that the pressure level reduces (becomes more negative) compared to the original model. As a consequence, the lift coefficient reduces in the present approach. It seems that the model is strongly influenced by the pressure gradient. For example, at $\alpha = 14°$ the deviation starts to occur downstream of the minimum Cp not only within the separated flow region.

In Figures 9c and 9d, the corresponding skin friction coefficient distributions are shown. It can be observed that the model again resembles the original SST model at a small angle of attack where the pressure gradient is small and no separation occurs (Figure 9c). From Figure 9d, a strong deviation of C_f starts to occur just downstream of the transition point while this is
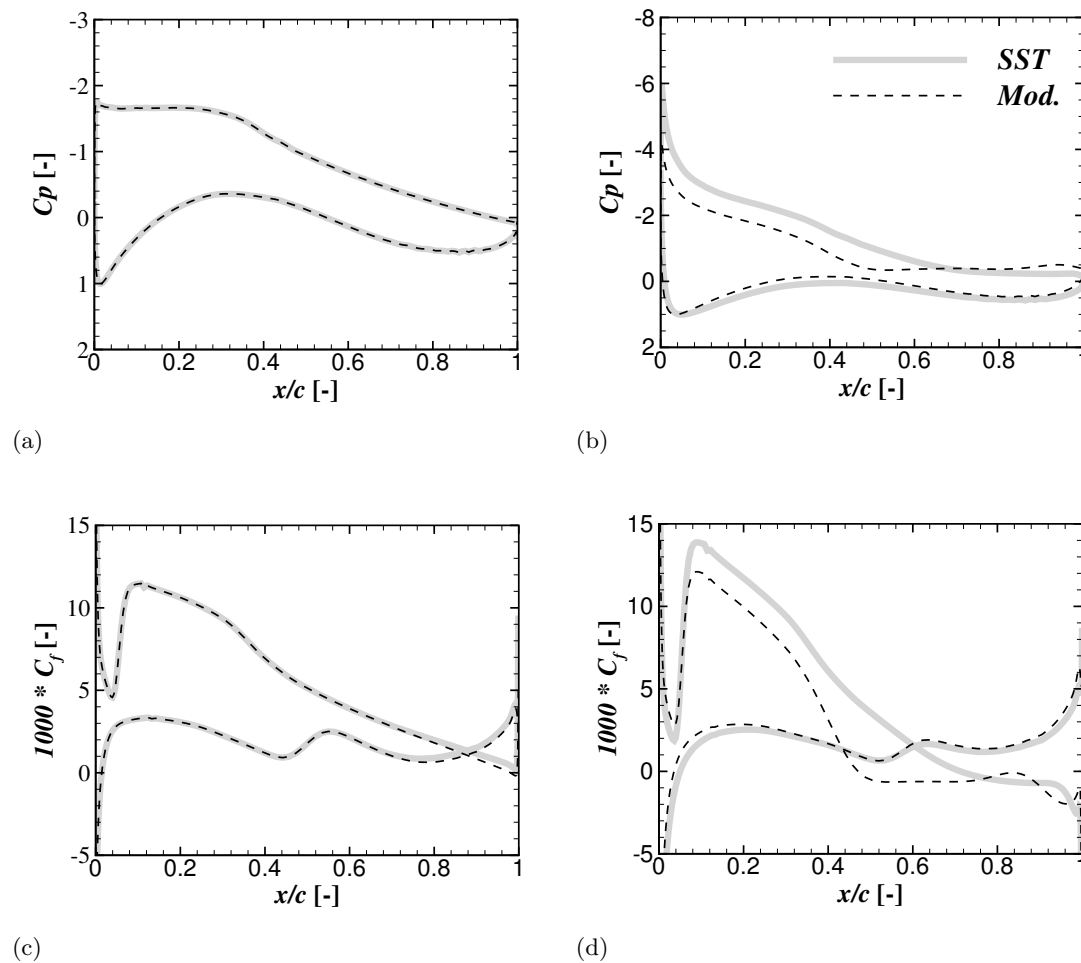

Figure 9: Predicted pressure and skin friction coefficients of the DU 91-W2-250 airfoil at $\alpha = 6°$ (left) and at $\alpha = 14°$ (right).

less prominent for the laminar portion of the flow ($x/c < 5\%$). The modified model reduces the magnitude of friction contribution compared to the original model. Furthermore, significantly earlier separation is observed as well (where $C_f < 0$). Within the separated flow area, the wall shear stress seems to be constant over a relatively large portion of the chord especially on the suction side.

Figure 10 presents the flow field around the airfoil at $\alpha = 14°$. It is shown clearly that stronger separation is observed for the present model compared to the Menter SST. The separated flow area starts from $x/c \approx 0.5$ for the present model, while it is further downstream for the Menter SST model from $x/c \approx 0.7$. The predicted separated flow area obtained by the present modification is expected to better represent the experiment because the error in the lift prediction is only 13.6%, compared to the original model that reaches 58.7% at this specific angle of attack.

To better understand the origin of the improvement, the velocity profile comparison is shown in Figures 11 and 12 for $x-$ and $y-$velocity components, respectively. The profiles are extracted from the velocity field in Figure 10 at five chordwise positions, namely $x/c = 0.1$, 0.25, 0.5, 0.75 and 0.9. It can be seen that the streamwise velocity profile well resembles the original SST model upstream of the separation point in Figures 11a and 11b. However, as separation starts to occur at $x/c = 0.5$, the velocity profile deviates showing a significant reduction of u^+ up to $y^+ < 253$. It shall be noted that no separation takes place for the original SST model at this position. The strongest deviation between the two models is observed at $x/c = 0.75$ in Figure 11d. Further downstream, the Menter SST model predicts strong flow separation that the difference between the models reduces.

A similar behaviour is observed also for the logarithmic $y-$velocity profiles in Figure 12. No deviation of the velocity profile is observed before separation takes place. A positive $y-$velocity component is observed for the modified model starting from $x/c = 0.5$ due to backflow. This phenomenon is observed also at $x/c = 0.75$ and 0.9 in Figures 12d and 12e, respectively. The positive v^+ magnitude is shown for the Menter SST model from $x/c = 0.75$. Despite that, the backflow is not as strong as for the modified model.

Figure 13 displays the Reynolds stress components from the turbulence models at the
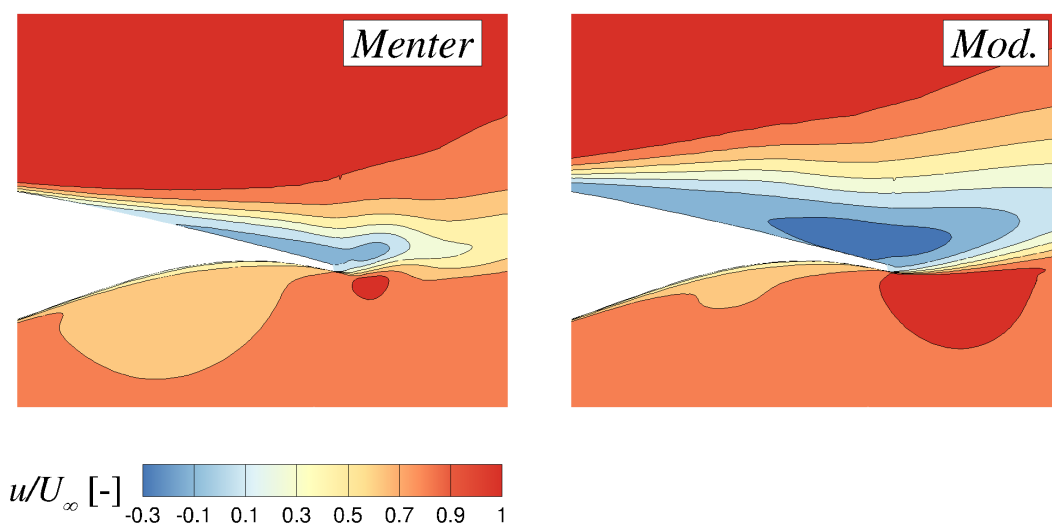

Figure 10: Predicted velocity field of the DU 91-W2-250 airfoil at $\alpha = 14°$. Stronger separation is predicted by the present model.

corresponding positions as the velocity profiles in Figures 11 and 12. Three different components are observed: $- < u'u' >$, $- < u'v' >$ and $- < v'v' >$. The Reynolds stresses are estimated by:

$$ - < u_i' u_j' > = \mu_t \left(\frac{\partial u_i}{\partial x_j} + \frac{\partial u_j}{\partial x_i} \right). \tag{16} $$

It shall be noted that the contribution of w remains zero since the simulations are two dimensional.

The $- < u'u' >$ plots are illustrated in Figures 13a-13d, $- < u'v' >$ in Figures 13e-13h and $- < v'v' >$ in Figures 13i-13l. The variable is normalized by the square of friction velocity (u^{*2}).

The plots again support the observation for the velocity profiles. It can be seen that both

(a)

(b)

(c)

(d)

(e)
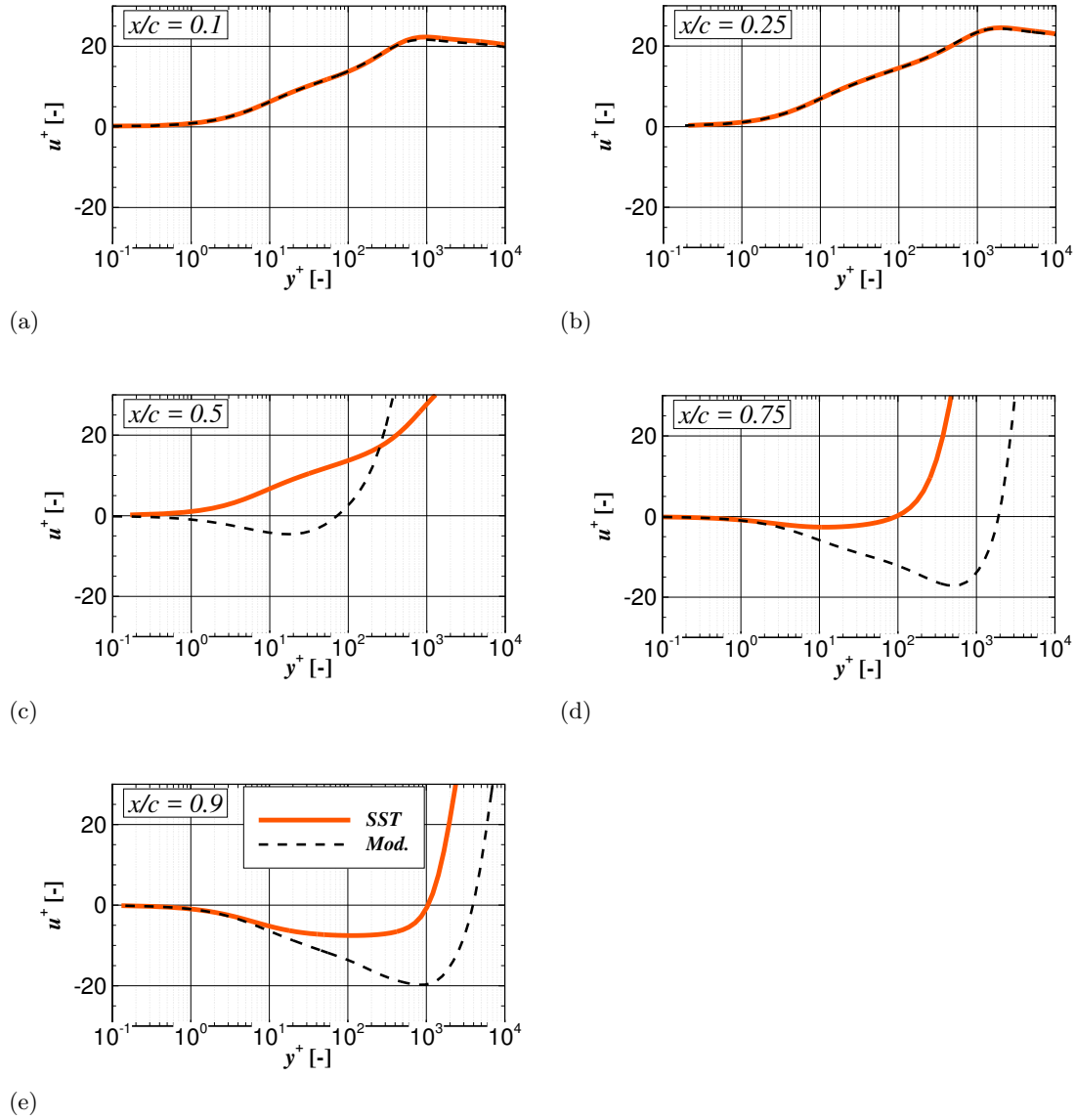
Figure 11: Nondimensional logarithmic $x-$velocity profiles on the suction side of the DU 91-W2-250 airfoil at $\alpha = 14°$. Dashed and solid lines represent the modified and the Menter SST models, respectively.

turbulence models have the similar prediction at $x/c = 0.25$ where no separation occurs. A small deviation is shown starting from $x/c = 0.5$. It becomes notable that the cross-contribution between $x-$ and $y-$velocity ($- < u'v' >$) is stronger than $- < u'u' >$ and $- < v'v' >$. Downstream of this position, the Reynold stresses are considerably different. The Reynolds stresses are damped near the wall up to a certain y^+ value for the modified model compared to the fuller profile for the original SST model. As a consequence, the stability of the flow to withstand the adverse pressure gradient becomes smaller, resulting in stronger separation. The damped area seems to increase with increasing x/c. For example, the Reynolds stresses are damped up to $y^+ = 1000$ for $x/c = 0.75$ but it reaches $y^+ = 2500$ for $x/c = 0.9$. It is shown, however, that the Reynolds stresses from the modified model are stronger at a larger y^+ value
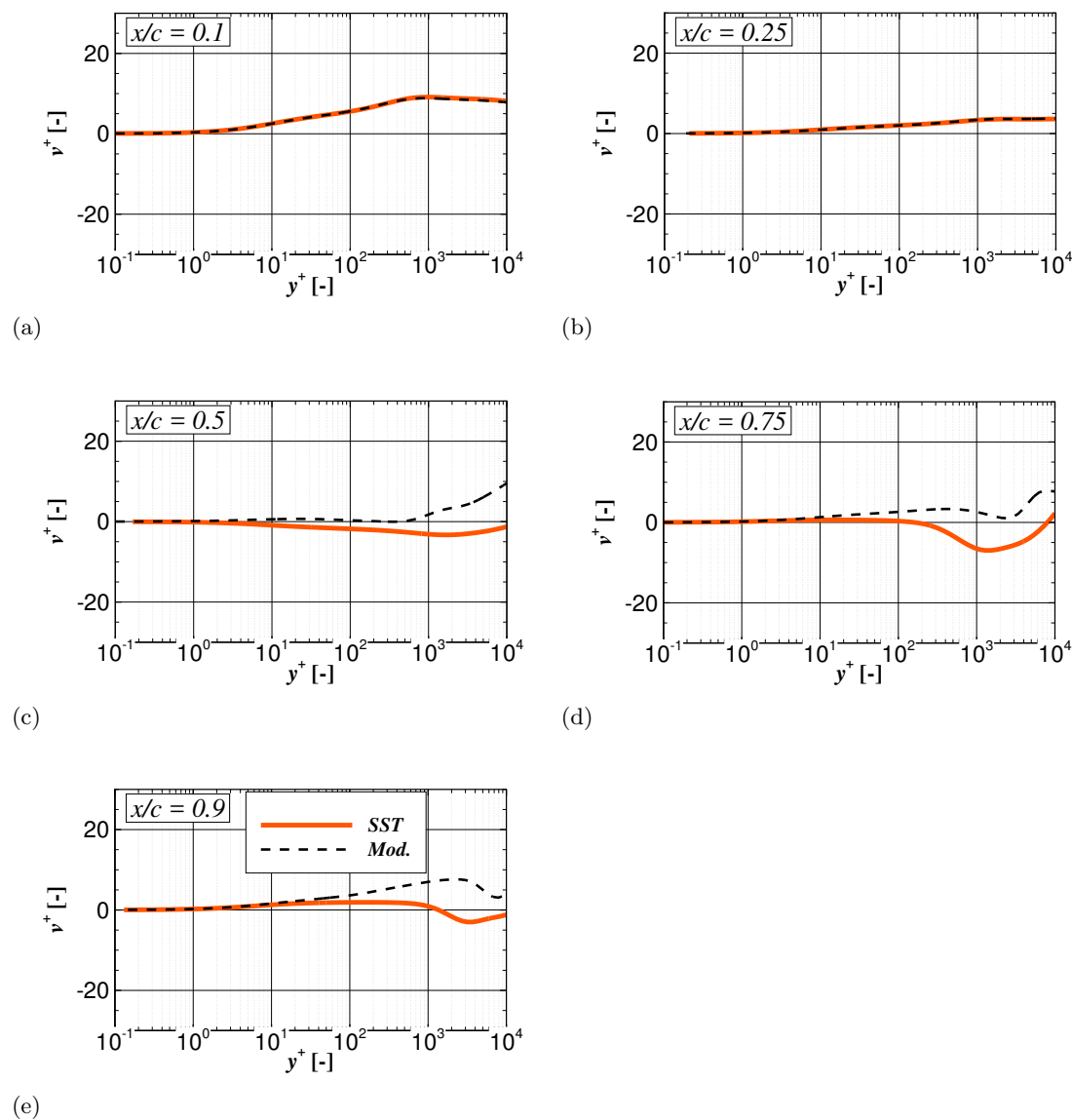

Figure 12: Nondimensional logarithmic $y-$velocity profiles on the suction side of the DU 91-W2-250 airfoil at $\alpha = 14°$. Dashed and solid lines represent the modified and the Menter SST models, respectively.
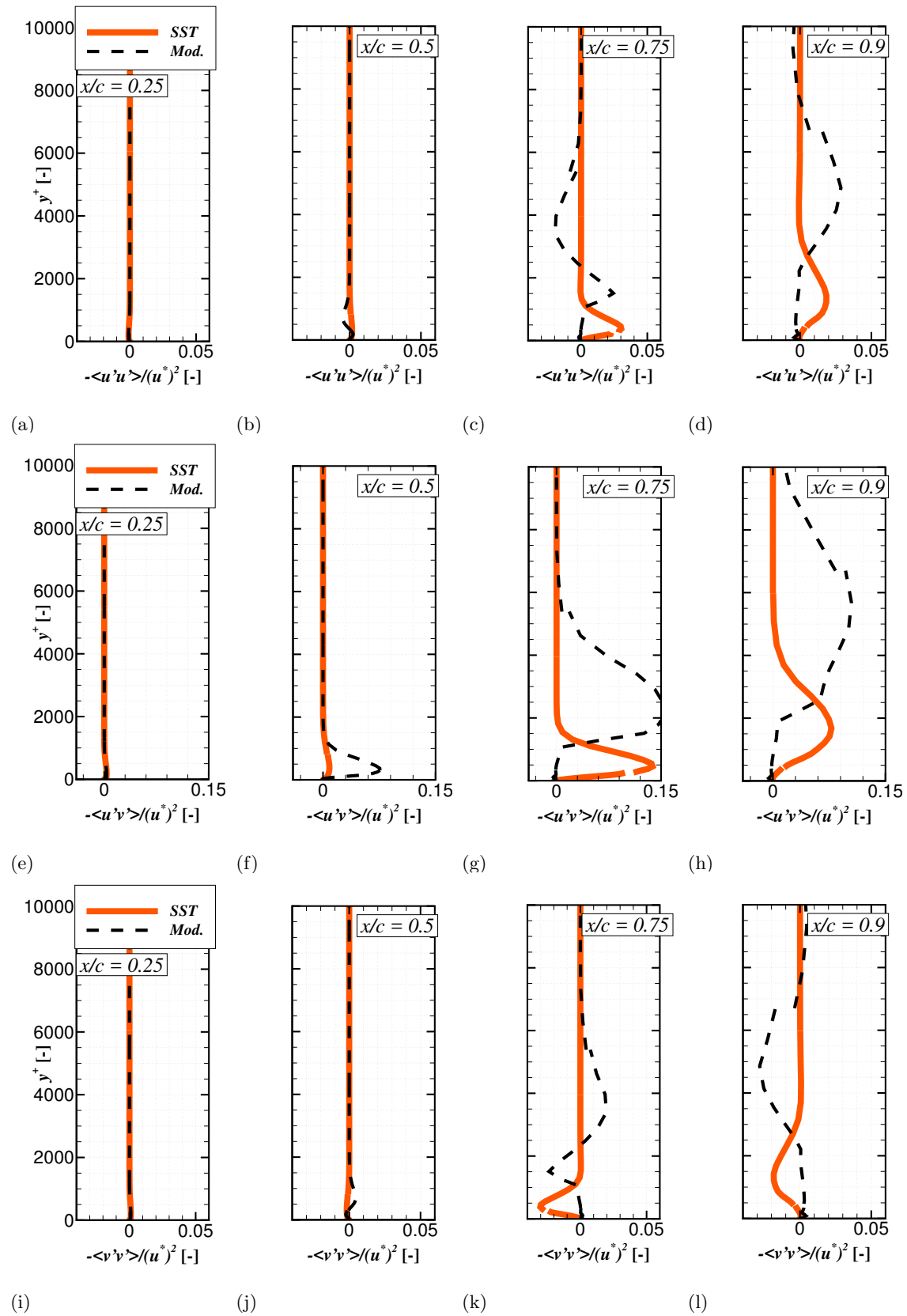
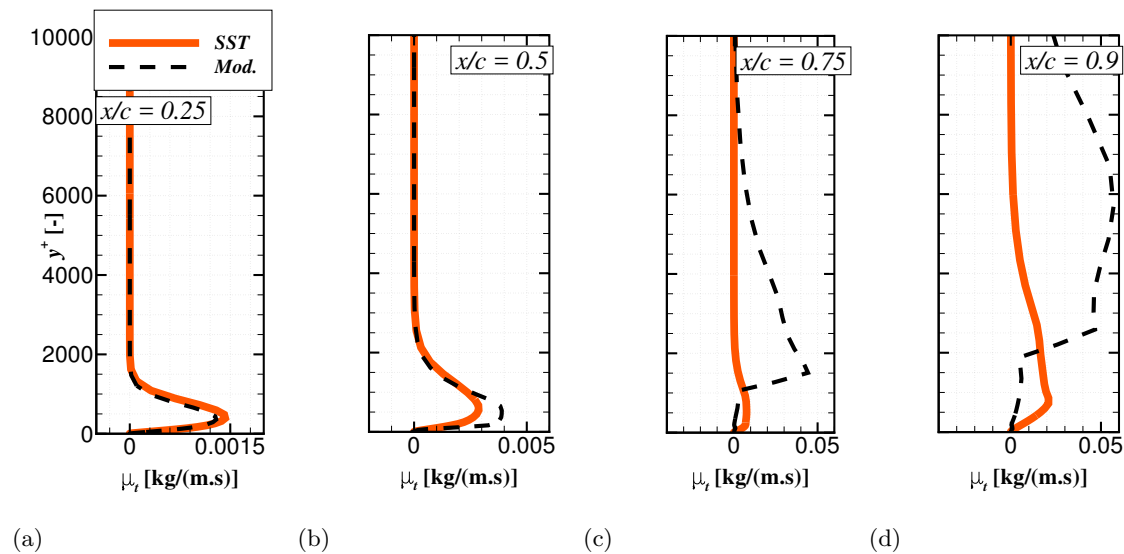Figure 13: Reynolds stresses from the computed by turbulence models.

Figure 14: Reynolds stresses from the computed by turbulence models.

than the damped area. This seems to be related to the displacement effect of the flow due to separated vortex up to the boundary layer edge. For example, the Reynolds stress terms increase up to around $y^+ = 9500$ (wall distance of about $0.18c$) at $x/c = 0.75$ while the boundary layer edge is at around $y^+ = 7000$.

The behaviour of the Reynolds stresses are strongly influenced by the turbulent viscosity magnitude. It is shown that the turbulent viscosity resembles the original SST model as long as no separation occurs. The effects of the damping factor are clearly displayed especially in Figures 14c and 14d. A sharp change of μ_t is shown since a step function model is used in the present works. But the influence of this sharp change seems to be minor because the Reynolds stresses profiles are still relatively smooth as already shown in Figure 13.

4. Conclusion and outlook
Computational Fluid Dynamics (CFD) studies have been performed on four thick wind turbine airfoils, namely DU 91-W2-250 (25% relative thickness), DU 97-W-300 (30%), DU 00-W2-350 (35%) and DU 00-W2-401 (40%). The simulations were carried out by employing the adjusted Menter SST turbulence model. The equation of the turbulent viscosity was redefined by adding a damping factor (f_b) to damp the turbulence. The damping factor was applied at regions near the wall controlled by a wall distance constant (w_d). Parametric studies were carried out to evaluate the sensitivity of the CFD results towards variation of the damping factor and wall distance constant. The results were evaluated and compared with the original Menter SST turbulence model and available measurement data to assess the accuracy of the model.

The evaluations show that the modified model is able to improve the CFD prediction especially at high angles of attack. The maximum lift coefficient and post stall characteristics are better captured even though the stall angle is not accurately predicted, which is expected due to three dimensionality and unsteadiness of the flow. The use of 3D CFD computations or eddy resolving technique like Large Eddy Simulations (LES) and Detached-Eddy Simulations (DES) may improve the situations. Nevertheless, both the models agree fairly well in the linear lift regime. At high angles of attack, the minimum pressure coefficient becomes more positive in the present model, increasing the pressure level on the suction side. On the other hand, the

pressure level reduces on the pressure side of the airfoil. As a result, the lift coefficient alleviates, reducing the lift error with the measurement data to 13.6% compared to the SST model that reaches 58.7%. Stronger separation is observed for the present model. The logarithmic velocity profile of the modified model well resembles the original SST model in the region where no separation occurs. The deviation between the the velocity profiles predicted by both models are noticeable within the separation area, indicating that the modification is activated. These phenomena are caused by the a strong reduction of the Reynolds stresses contribution near the wall that makes the flow becomes more vulnerable towards the adverse pressure gradient especially at high angles of attack.

In the present studies, only two dimensional simulations were carried out. It is suggested to examine the performance of the model for three dimensional flow. Applying the model using the full 3D Navier-Stokes computations on wind turbine rotors are strongly recommended. Furthermore, the present model can be used as the near wall RANS model for the DES approach to improve the prediction of separation within the boundary layer flows. The model is, however, not yet tested for rotating coordinate system since the objective of the present studies is to improve the prediction of the model for generating airfoil databases used by BEM simulations. Further investigations regarding this aspect are recommended.

Acknowledgements

References
[1] Rhie C and Chow W 1983 *AIAA journal* **21** 1525–1532
[2] Bangga G, Lutz T, Jost E and Krmer E 2017 *Journal of Renewable and Sustainable Energy* **9** 023304 URL http://dx.doi.org/10.1063/1.4978681
[3] Duque E P, Burklund M D and Johnson W 2003 *Journal of Solar Energy Engineering* **125** 457–467
[4] Pape A L and Lecanu J 2004 *Wind Energy* **7** 309–324
[5] Bangga G, Lutz T and Krämer E September 23-25, 2015 *EAWE PhD Seminar 11* (Stuttgart, Germany)
[6] Bangga G, Lutz T and Krämer E May 19-20, 2015 *Proceedings of German Wind Energy Conference 12, DEWEK 2015* (Bremen, Germany)
[7] Kim Y, Jost E, Bangga G, Weihing P and Lutz T 2016 *Journal of Physics: Conference Series* vol 753 (IOP Publishing) p 032047 URL https://doi.org/10.1088/1742-6596/753/3/032047
[8] Shur M, Spalart P, Strelets M and Travin A 1999 *Engineering turbulence modelling and experiments* **4** 669–678
[9] Bangga G, Weihing P, Lutz T and Krämer E 2017 *Journal of Mechanical Science and Technology* **31** 2359–2364 URL http://dx.doi.org/10.1007/s12206-017-0432-6
[10] Bangga G, Lutz T and Krämer E 2017 *Journal of Mechanical Science and Technology* **31** 3839–3844 URL http://dx.doi.org/10.1007/s12206-017-0728-6
[11] Bangga G, Weihing P, Lutz T and Krämer E 2018 *Hybrid RANS/LES simulations of the three-dimensional flow at root region of a 10 MW wind turbine rotor. New Results in Numerical and Experimental Fluid Mechanics XI* (Springer) pp 707–716 URL http://dx.doi.org/10.1007/978-3-319-64519-3_63
[12] Bangga G, Guma G, Lutz T and Krämer E 2018 *Wind Engineering* (To be published)
[13] Myong H K and Kasagi N 1990 *JSME international journal. Ser. 2, Fluids engineering, heat transfer, power, combustion, thermophysical properties* **33** 63–72
[14] Menter F R 1994 *AIAA journal* **32** 1598–1605
[15] Wilcox D C *et al.* 1998 *Turbulence modeling for CFD* vol 2 (DCW industries La Canada, CA)
[16] Launder B E and Spalding D B 1972
[17] Nagano Y and Hattori H 2001 *TSFP DIGITAL LIBRARY ONLINE* (Begel House Inc.)

[18] Chitsomboon T and Thamthae C 2011 *Proceedings of the World Renewable Energy Congress* vol 15 pp 4114–4120

[19] Bangga G 2013 *Assessment of modified two-equations U-RANS turbulence model to predict the onset of dynamic stall* Master's thesis Institut Teknologi Sepuluh Nopember

[20] Bangga G and Sasongko H 2017 *Journal of Applied Fluid Mechanics* **10** 1–10 URL https://doi.org/10.18869/acadpub.jafm.73.238.26391

[21] Wilcox D C 1993 *AIAA journal* **31** 1414–1421

[22] Ansys A F 2011 *ANSYS inc* 218–221

[23] Kroll N, Rossow C C, Becker K and Thiele F 2000 *Aerospace Science and Technology* **4** 223–237

[24] Aumann P, Bartelheimer W, Bleecke H, Kuntz M, Lieser J, Monsen E, Eisfeld B, Fassbender J, Heinrich R and Kroll N, Mauss M, Raddatz J, Reisch U, Roll B, Schwarz T 2008 *FLOWer installation and user manual* Deutsches Zentrum fur Luft- und Raumfahrt

[25] Schwarz T, Spiering F and Kroll N 2010 *Second Symposium of Simulation of Wing and Nacelle Stall*

[26] Bangga G, Kim Y, Lutz T, Weihing P and Krämer E 2016 *Journal of Physics: Conference Series* **753** 022026 URL https://doi.org/10.1088/1742-6596/753/2/022026

[27] Bangga G, Lutz T, Dessoky A and Krämer E 2017 *Journal of Renewable and Sustainable Energy* **9** 053303 URL http://dx.doi.org/10.1063/1.5003772

[28] Jameson A, Schmidt W, Turkel E *et al.* 1981 *AIAA paper* **1259** 1981

[29] Jameson A 1991 *AIAA paper* **1596** 1991

[30] Radespiel R, Rossow C and Swanson R 1990 *AIAA journal* **28** 1464–1472

[31] Timmer W and Van Rooij R 2003 *Journal of Solar Energy Engineering* **125** 488–496

[32] Van Rooij R and Timmer W 2003 *Journal of solar energy engineering* **125** 468–478

[33] Drela M 1989 *Low Reynolds number aerodynamics* (Springer) pp 1–12

[34] Lekou D, Chortis D, Chaviaropoulos P, Munduate X, Irisarri A, Madsen H, Yde K, Thomsen K, Stettner M and Reijerkerk M, Grasso F, Savenije R, Schepers G, Andersen CF 2015 Avatar deliverable d1.2 reference blade design Tech. rep. ECN Wind Energy

[35] Wieghardt K and Tillmann W 1951

[36] Bangga G, Hutomo G, Wiranegara R and Sasongko H 2017 *Journal of Mechanical Science and Technology* **31** 261–267 URL http://dx.doi.org/10.1007/s12206-016-1228-9

[37] Fröhlich J and von Terzi D 2008 *Progress in Aerospace Sciences* **44** 349–377

2018-04-30

Improving a two-equation eddy-viscosity turbulence model to predict the aerodynamic performance of thick wind turbine airfoils

Bangga, Galih

IOP